Available online at www.eccomasproceedia.org
Eccomas Proceedia SMART (2023) 250-261

ECCOMAS
Proceedia

X ECCOMAS Thematic Conference on Smart Structures and Materials
SMART 2023
D.A. Saravanos, A. Benjeddou, N. Chrysochoidis and T. Theodosiou (Eds)

ON THE FUNCTIONALIZATION OF COMPOSITE STRUCTURES USING PIEZOELECTRIC TRANSDUCERS FOR TRANSPORTATION APPLICATIONS: VIBRATION CONTROL AND ENERGY HARVESTING

Jonathan Rodriguez*, Linjuan Yan†, Kevin Billon‡, Mickael Lallart†, Manuel Collet‡, Simon Chesne*

*Univ Lyon, INSA Lyon, CNRS, LaMCoS, UMR5259
69621 Villeurbanne, France
e-mail: jonathan.rodriguez@insa-lyon.fr

† Univ. Lyon, INSA-Lyon, LGEF EA 682, F-69621 Villeurbanne, France

‡ Univ. Lyon, Ecole Centrale de Lyon, LTDS UMR CNRS 5513, F-69134 Ecully, France.

Abstract. Composite material parts are used more than ever in transportation applications due to their lightweight and mechanical strength. In recent years, progresses in additive manufacturing processes have allowed not only to produce such materials more easily but also to integrate active components inside the layers to create smart composite materials. This paper presents two concrete applications for the transportation field using integrated piezoelectric transducers inside the composite material layers: energy harvesting for embedded sensors and vibration control. First, a composite reduced-model car with an integrated transducer is excited using a roller test bench. The piezoelectric patch is then coupled with an optimized self-powered Synchronized Switch Harvesting on Inductor circuit (SSHI) and up to 40μW are harvested on a resistive load. This power is stored on a capacitor and used to supply a temperature sensor in addition to its wireless transmitter. The second application is the control of vibrations through multiple transducers as actuators and sensors integrated directly into the composite material of a spoiler using also nonlinear switching methods like Sliding Mode Control. The performance level achieved on the targeted modes is up to -22dB, illustrating the potential of nonlinear switching control for vibration control. These two applications provide good illustrations of the promising capabilities in the transportation field of integrated composite smart structures.

Key words: Smart Structures, Piezoelectric Materials, Energy harvesting, Vibration control

Peer-review under responsibility of the organizing committee of SMART 2023.
doi: 10.7712/150123.9782.442379

1 INTRODUCTION

Composite structures have shown over recent years great potential specifically in transportation thanks to their lightweight and excellent mechanical properties. Now by integrating properly piezoelectric transducers directly into the composite layers, composite smart structures can sense strain for structural health monitoring [1], apply certain stress for dynamics or noise control [2], but also retrieve electrical energy to supply low-power electronics [3].

Considering first the energy harvesting process using integrated piezoelectric transducers, their efficiency in energy conversion still remains a technological difficulty. The host structure shape and material in addition to the mounting of the piezoelectric transducers is not always optimal and can lead to weak electromechanical coupling. To overcome such challenges, energy harvesting systems are generally designed to benefit from dynamic amplifications in the structure response. Nevertheless, in an operational environment, the mechanical perturbation does not always excite the main structural modes which significantly reduces the efficiency of the harvesting process. One promising solution to enhance the harvested energy is to optimize the interface circuit between the transducers and the charging capacitance. Thus, [4] and [5] investigated Synchronized Switching Harvesting on Inductor (SSHI) circuits to take advantage of a switching inversion process triggered when the strain in the transducer reaches an extremum. Thanks to this switching action and even in the case of weakly coupled structures, harvested power can gain up to a decade compared to Standard Energy Harvesting circuits (SEH).

Secondly, if the use of nonlinear methods for energy harvesting applications provides better performance and especially robustness, it is also the case within the field of dynamics control. Thus, sliding mode control (SMC) [6] gained interest in the last decade thanks to its robustness. The principle is to define a sliding surface, as a function of the error vector, and then design a switching control signal based on the defined sliding variable. The closed-loop dynamics are then constrained to those of the sliding variable and driven to converge to the sliding surface. A wide variety of SMC controllers have been investigated since but few are applied to vibration control problems [7, 8] and even fewer to smart structures with piezoelectric transducers [9].

This manuscript presents two practical applications of composite smart structures for energy harvesting and dynamics control where the performance gain using nonlinear switching methods are highlighted. This short paper is organized as follows: Section 2 introduces the energy harvesting application on an RC car smart composite body and Section 3 develops the vibration control application.

2 ENERGY HARVESTING APPLICATIONS ON WEAKLY COUPLED STRUCTURES

The present section develops the energy harvesting application on the RC car smart composite body where the final objective is to supply a temperature sensor with its wireless transmitter.

2.1 The smart composite car body

The first composite structure is a reduced-model car body (scale 1/12) manufactured by the M3M laboratory (UTBM - France) in fiberglass. 5 piezoelectric transducers of 25mm diameter,

$150\mu m$ thickness, and 34nF nominal capacitance (piezoceramic patches from Murata) are integrated inside the fibers during the manufacturing process. Due to electromechanical coupling considerations, only one transducer will be considered here for the energy harvesting application. Figure 1 shows a picture of the experimental setup and schemes of the experiment principle. Thus, the modified body is fixed to the original RC car chassis and placed on a roller test bench where the vehicle's electric motor is supplied with a constant voltage input. Hence, the car moves on the rollers, and vibrations are transmitted to the composite body through contact with the tires.

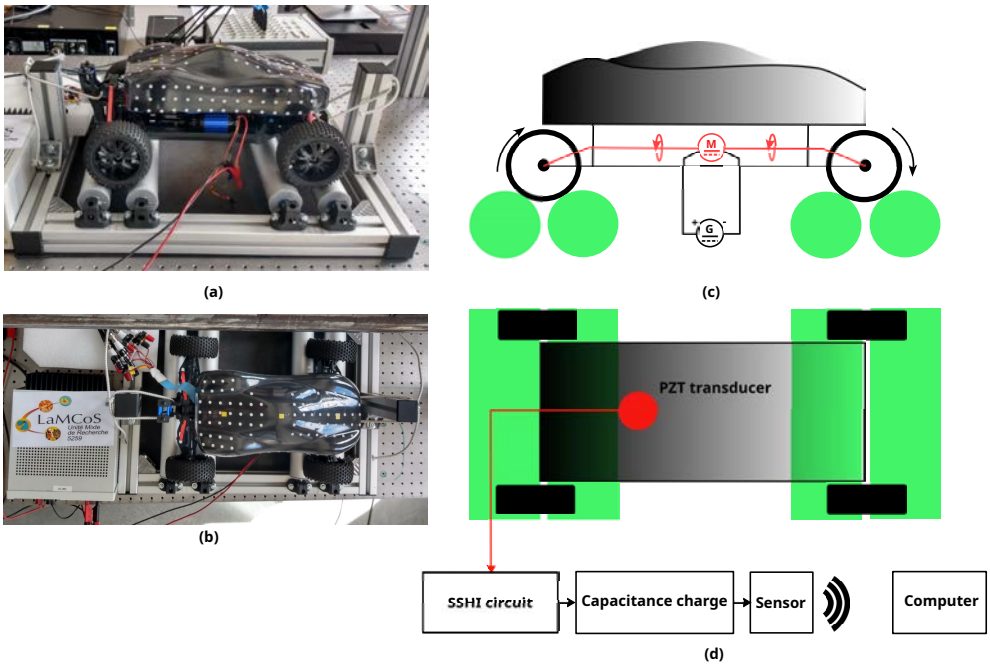

Figure 1: Smart composite car body with chassis and roller test bench: (a) side view, (b) top view, (c) actuation components, (d) energy harvesting process.

2.2 Structural response to road excitation

Since the available electrical energy for depends on the piezoelectric voltage U_{PZT} response to the roller excitation, it is possible to determine an optimal vehicle velocity *i.e* electric supply voltage to the DC motor. Thus, U_{PZT} is measured at a sampling frequency of 10kHz for different vehicle velocities corresponding to a motor supply voltage U_{EM} value from 1V to 3.6V (5 to $18km.h^{-1}$). Figure2(a) shows the power spectral density of each measured time signal U_{PZT} and highlights that major part of the electrical energy generated by the integrated piezoelectric transducer is located at motor velocity-dependent frequencies. Hence, the main source of strain comes from the contact between the tires and the rollers, not the modal behavior of the composite body. Figure 2(b) displays the total energy of the considered transducer output voltage

and its dependence on the vehicle velocity. The optimal supply voltage of the electric motor is 3V corresponding to a vehicle velocity of $14.7 km.h^{-1}$. At this velocity, the most energetic harmonic frequencies in the voltage signal U_{PZT} are 22, 44, and 66Hz.

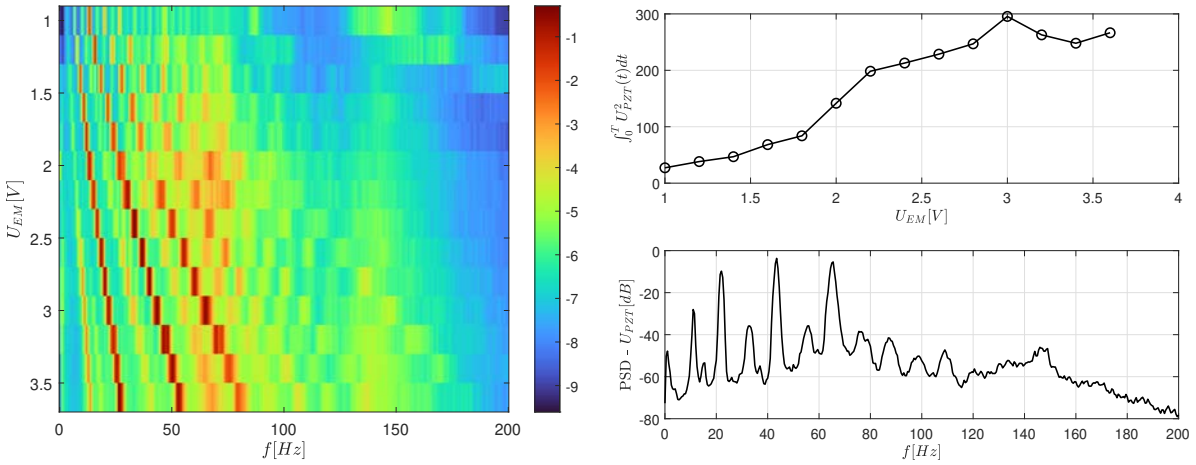

(a) (b)

Figure 2: (a) Power spectral density of U_{PZT} in function of the electric motor supply voltage U_{EM}, (b) corresponding energy of the signal U_{PZT} (top) and PSD of the transducer output voltage at optimal velocity (bottom).

From the observation of the system response, one can notice that it has no major modal response at low frequencies due to its complex shape providing high rigidity. This situation represents the most challenging case for energy harvesting applications since the structure has not been pre-optimized to enhance local strain at particular frequencies.

2.3 SSHI circuit

Since the transducer output voltage signal is non-sinusoidal and has also a reduced amplitude, an optimized electronic circuit must be set between the transducer and the load (capacitance to charge). Hence, a SSHI circuit is placed between the transducer and a full wave voltage doubler as shown in Figures 3(a) and 3(b) to amplify the available electrical energy before the rectifier. Figure 3(c) details the principles of the SSHI circuit taking as example a sinusoidal voltage signal. The inductance L coupled with the capacitance of the transducer forms an oscillating circuit. As the switch SW is closed, the voltage oscillates around 0. After half an oscillation, the piezoelectric voltage reaches an extremum and the switch SW opens, realizing a voltage inversion operation. Thanks to this process, a cumulative voltage amplification occurs and up to a decade higher in available power can be reached under the condition of pure sinusoidal strain. However, since the inversion process brings losses due to the resistive parts, the efficiency might be reduced. The SSHI method is particularly well adapted for smart structures with low electromechanical coupling or broadband excitation signals thanks to its functional robustness and

adaptiveness. In addition, the switching operation with the extremum detection is completely self-powered in this application, thereby reducing the energy losses in the circuit.

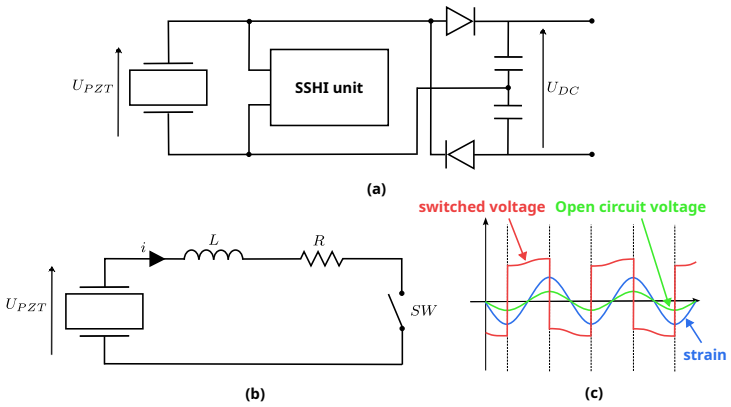

Figure 3: Smart composite spoiler: (a) picture of the experimental setup, (b) side view of the spoiler with the 6 PZT transducers, (c) top view of the spoiler with depiction of each PZT role.

2.4 Experimental results

Figure 4(a) shows the output voltage of the transducer in open circuit and with the SSHI circuit without rectifier or load for a motor supply voltage of 2.56V. Thanks to the switching process, the output voltage RMS value is increased from 1.62V to 3.83V representing a gain of 2.4.

The optimal load is now determined for the SEH circuit: 1MΩ and the SSHI circuit: 3MΩ. The global output power is compared on both harvesting devices in Figure 4(b) for different velocities. At low speed, the voltage amplitude is not sufficient to trigger the self-powered switching device. However, with the speed and the mechanical excitation increasing, the output power is amplified through the SSHI circuit by a factor superior to 2 reaching a harvested power of 40μW.

Considering such magnification, a STM 330 module from Enocean GmbH is now connected to the circuit, including an embedded temperature sensor. To assess properly the self-powering capabilities of the circuit, the battery of the module and its photovoltaic cell are removed. Considering an average supply voltage of 3V and transmission of the temperature measurement every 60s, the power consumption is estimated at 8μW which is compatible with the available harvested power from the SSHI circuit. Hence, the total system should be energetically viable from a minimum velocity of 8.5 km.h^{-1} while the necessary velocity for SEH is 10km.h^{-1}. Finally, the equivalent storage capacitance associated with the system is 705μF.

For the final experimental validation of the self-powered sensor and transmitter, the system starts with null initial state $i.e.$ vehicle at 0 velocity and all capacitors discharged. First, a constant velocity command of 12.52 km.$^{-1}$ is applied to the RC car on the roller test bench, and Figure 4(c) displays the rectified voltage supplying the sensor in the time domain. After an

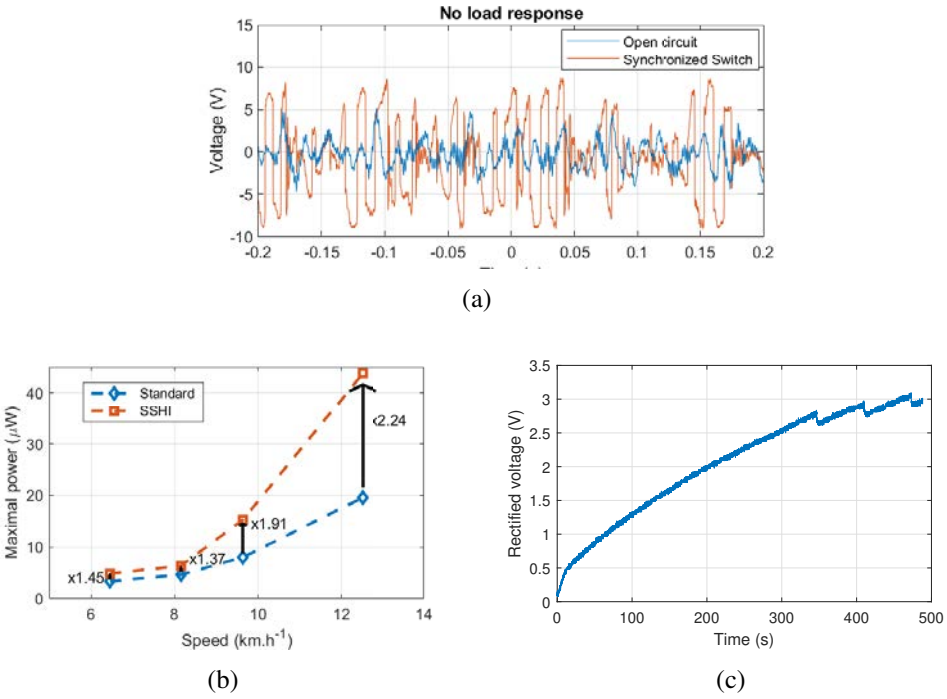

(a)

(b)

(c)

Figure 4: From [10] : (a) open circuit voltage U_{PZT} and rectified voltage after the switch, (b) experimental power as a function of car velocity on optimal load for SEH and SSHI circuit, (b) rectified voltage supplying the sensor from zero. initial conditions .

exponential charge up to 2.8V in 345s, the system starts to transmit data every 60s to the wireless receiver, maintaining an average voltage of 3V. Two different data transmission systems are then successfully tested. The first is using a USB 300 gateway from EnOcean GmbH connected to a computer equipped with DophinView software. The second one, more relevant for embedded applications, is based on an EnOcean Pi radio module connected to an M5Stack Core2 module (featuring ESP32 System on Chip).

Thus, from a weakly coupled electromechanical system excited by non-monochromatic disturbance, it still has been possible to supply a sensor and its wireless transmission module. This application of integrated piezoelectric transducers illustrates how smart composite structures can be completely autonomous and fully integrated into their self-sensing capabilities, especially in transportation since vibrations are unconditionally present.

3 STRUCTURAL CONTROL APPLICATIONS

The following section develops a dynamics control application on a smart composite spoiler using nonlinear modal control.

3.1 The smart composite spoiler

The second smart structure is a composite spoiler of 1150×300×25 in fiberglass also manufactured by the M3M laboratory with a 3 layers architecture. 48 of the same PZT transducers from the composite smart body car are distributed into the composite layers of the spoiler. For this study, only 6 PZT transducers are considered within the vibration control loop: 1 for the disturbance input, 3 sensors, and 2 control actuators. Figure 5 displays the experimental setup and position of each transducer with its role. The spoiler is suspended with low stiffness elements and for the real-time control loop, a dSpace control unit is used.

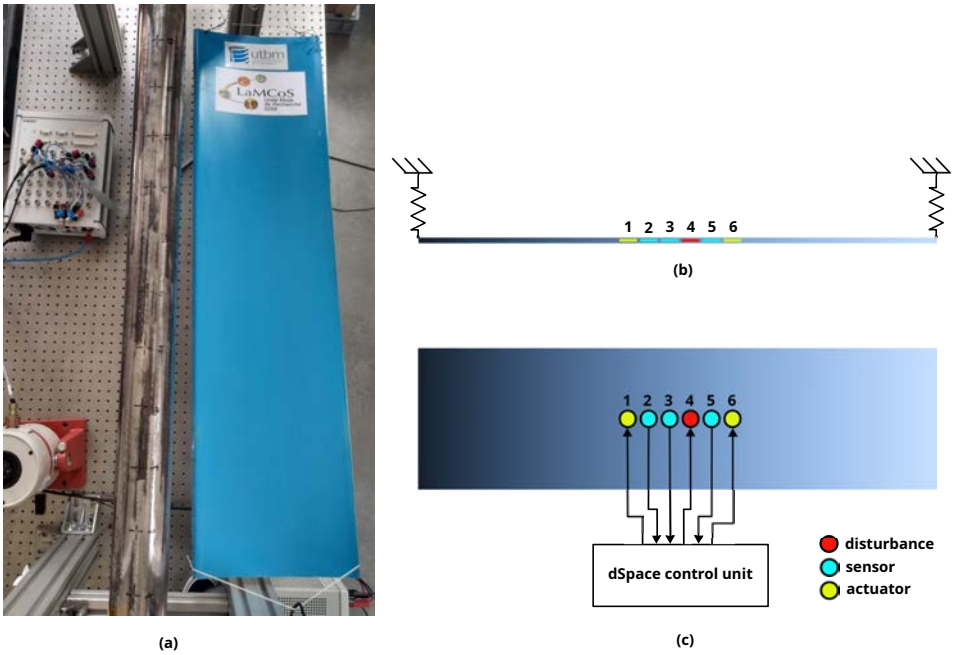

Figure 5: Smart composite spoiler: (a) picture of the experimental setup, (b) side view of the spoiler with the 6 PZT transducers, (c) top view of the spoiler with depiction of each PZT role.

3.2 Structural response and identification

Let us now define $H_{k,l}$ the transfer function between the PZT actuator l voltage input and the PZT sensor k voltage output with $l = 1, 6$ and $k = 2, 3, 5$. For the identification process, a white noise voltage signal is applied to each one of the actuators at a sampling frequency of 20kHz and a maximum amplitude of 3V. Figure 6 displays the amplitude of the six frequency response functions (FRF). Below 2kHz, 3 modes are observable in all the measured FRFs: 766Hz, 1282Hz, and 1576Hz. Assuming that each one of the previously identified n target modes is sufficiently separated from the others, the transfer function $H_{k,l}(s)$ can be written as a

sum of modal responses in the form:

$$H_{k,l}(s) = \sum_{i}^{n} \frac{a_i^{k,l} + b_i^{k,l} s}{s^2 + 2\xi_i \omega_i s + \omega_i^2} \tag{1}$$

where $s = j\omega$ is the Laplace variable, ω_i the mode frequency, ξ_i the modal damping ratio and $(a_i^{k,l}, b_i^{k,l}) \in \mathbb{R}^2$ are correction coefficients to obtain the correct magnitude and phase at the frequency of each mode. Through the extended procedure detailed in [11], a state space realization of the global MIMO system G is determined:

$$G \begin{cases} \dot{x} &= Ax &+ Bu \\ y &= Cx \end{cases} \tag{2}$$

with $x \in \mathbb{R}^{2n.N_a}$, $u \in \mathbb{R}^{N_a}$, $y \in \mathbb{R}^{N_s}$, $A \in \mathbb{R}^{2n.N_a \times 2n.N_a}$, $B \in \mathbb{R}^{2n.N_a \times N_a}$, and $C \in \mathbb{R}^{N_s \times 2n.N_a}$. N_s is defined as the number of sensors and N_a the number of actuators.

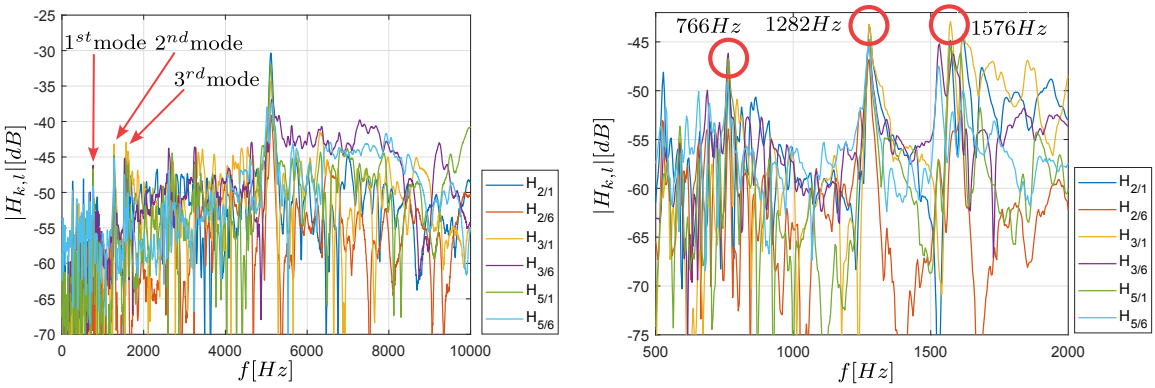

(a) (b)

Figure 6: (a) Frequency response function between the PZT actuators (1,6) and sensors (2,3,5) with the target modes control, (b) zoom on the bandwidth of interest.

3.3 Sliding mode control

Now that the system G including all the modeled dynamics of the transfer functions $H_{k,l}$ has a standard state-space representation, a modal-shaped sliding mode control is designed. This robust nonlinear control method, such as the SSHI circuit, uses a controlled switch to maintain the system onto the desired dynamics in the Filippov sense. A schematic representation of the control loop is shown in Figure 7. First, a pre- and post- filters defined respectively by $R^{-1/2}$ and $F^{1/2}$ are applied to the modeled plant G to enhance further the control energy on the desired modes such that:

$$R^{-1/2} \begin{cases} \dot{x}_R &= A_R x_R &+ B_R \bar{u} \\ u &= C_R x_R \end{cases} \qquad F^{1/2} \begin{cases} \dot{x}_F &= A_F x_F &+ B_F y \\ \bar{y} &= C_F x_F &+ D_F y \end{cases} \tag{3}$$

The augmented system containing the filters and the modeled dynamics G is defined with a new state vector $z = [x^T\ x_F^T\ x_R^T]^T$ and the following state space realization:

$$\begin{bmatrix} \dot{x} \\ \dot{x_F} \\ \dot{x_R} \end{bmatrix} = \begin{bmatrix} A & 0 & BC_R \\ B_F C & A_F & 0 \\ 0 & 0 & A_R \end{bmatrix} \begin{bmatrix} x \\ x_F \\ x_R \end{bmatrix} + \begin{bmatrix} 0 \\ 0 \\ B_R \end{bmatrix} \bar{u} \qquad \bar{y} = [D_F C\ C_F\ 0] \begin{bmatrix} x \\ x_F \\ x_R \end{bmatrix} \tag{4}$$

with $\bar{u} \in \mathbb{R}^{N_a}$ and $\bar{y} \in \mathbb{R}^{N_s}$ as the new system input and output. For the sake of simplicity, the new state-space realization (4) is defined as:

$$\begin{cases} \dot{z} &= \tilde{A}z &+ \tilde{B}\bar{u} \\ \bar{y} &= \tilde{C}z \end{cases} \tag{5}$$

where $\tilde{A} \in \mathbb{R}^{N \times N}$, $N \geq 2n + 2$, $\tilde{B} \in \mathbb{R}^{N \times N_a}$, $\tilde{C} \in \mathbb{R}^{N_s \times N}$. A switching function $\sigma \in \mathbb{R}^{N_a}$ is now defined such that $\sigma = Sz$ with $S \in \mathbb{R}^{N_a \times N}$ to be defined. The complete design procedure to optimally define S is detailed in [6]. Thus, a coordinate transform is applied to the augmented system to obtain a reduced-order model driven only by the dynamics of the sliding variable σ. At last, the so-called sliding motion of the closed-loop is expressed by $\sigma = \dot{\sigma} = 0$. From this condition and the system (5) comes the first term, linear, of the control signal:

$$\bar{u}_{eq} = -(S\tilde{B})^{-1} S\tilde{A}z \tag{6}$$

with $(S\tilde{B})$ being non singular by definition. Since the control $\bar{u}_{eq}$ is marginally stable, we define a positive definite and diagonal matrix $P \in \mathbb{R}^{m,m}$ with $m = rank(\tilde{B})$, satisfying the Lyapunov equation $P\Phi + \Phi^T P = -I$. Hence, the linear stable control part is defined as:

$$\bar{u}_{lin} = -(S\tilde{B})^{-1} \left(S\tilde{A} - \Phi S \right) z \tag{7}$$

Then, the nonlinear part of the control u_{nl} is designed:

$$u_{nl} = -\rho(S\tilde{B})^{-1} \frac{P\sigma}{||P\sigma||} \tag{8}$$

where $\rho \in \mathbb{R}^+$ and $\frac{P\sigma}{||P\sigma||}$ is a vector sign function. Therefore, it is not desirable to filter the switching control signal with $R^{-1/2}$ to maintain the robustness properties of SMC. u_{nl} is thereby directly applied to the physical plant G as in Figure 7. Stability of the nonlinear closed-loop is then guaranteed using the Kalman-Yakubovich-Popov theorem and designing the filter $R^{-1/2}$ to ensure the linear open-loop transfer function passivity. Besides, the nonlinear function $f(\sigma) = \frac{P\sigma}{||P\sigma||}$ is replaced for practical concerns by an approximation of the switching function as $\frac{P\sigma}{||P\sigma||+\epsilon}$ with $\epsilon << 1$.

Finally, the full-state x is necessary to compute the extended state vector z where the states of the filters $R^{-1/2}$ and $F^{1/2}$ are already known. Thus, a Kalman observer is designed to estimate x:

$$\dot{\hat{x}} \quad = \quad A\hat{x} + Bu + L\left(y - C\hat{x}\right) \tag{9}$$

where $\hat{x} \in \mathbb{R}^{2n}$ is the real state estimation.

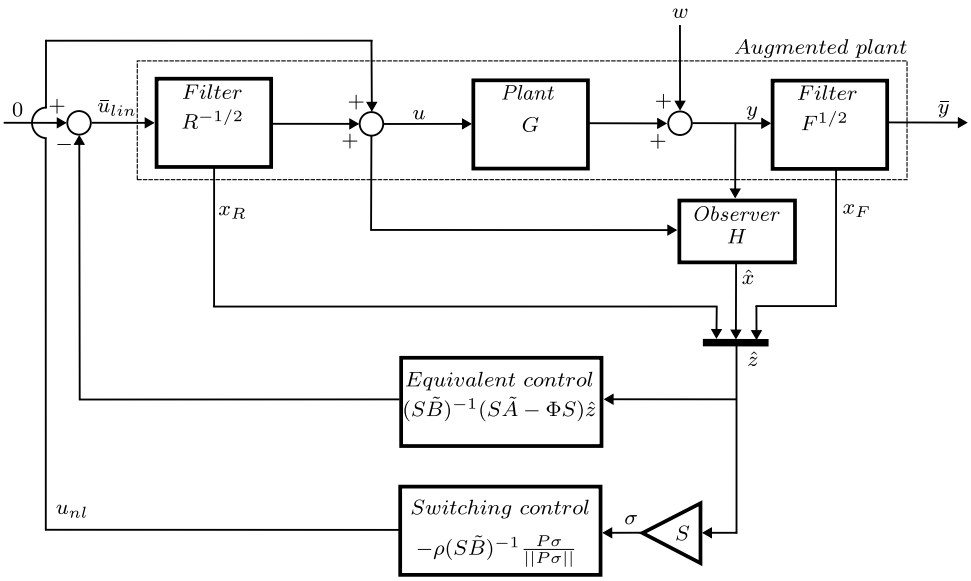

Figure 7: Linear and nonlinear closed-loop for switching control.

3.4 Experimental results

The following subsection develops the experimental results obtained and the reader can refer to [11] for more details about the controller parameters tuning. The disturbance applied to PZT 4 is the same signal used for the identification process. Figure 8 shows the power spectral density response for the PZT sensors 2, 3, and 5 for 4 configurations: without control, with linear control $\bar{u}_{lin}$ only, with switching control u_{nl} only, and finally with the complete SMC controller. It is clearly observable that the 2 integrated piezoelectric actuators manage to reduce drastically the strain amplitude for all PZT sensors, and for all the targeted modes with a reduction going from -16 to -22dB. It is interesting to notice that both linear and nonlinear parts of the control bring independently good vibration mitigation. However, both parts are complementary considering the control performance of the complete SMC.

	Voltage RMS value
Excitation - U_4	1.34
$U_{1,lin}$	0.2
$U_{6,lin}$	0.16
$U_{1,nl}$	0.83
$U_{6,nl}$	0.54
U_1	0.84
U_6	0.59

Table 1: RMS voltage values for excitation signal, linear control signals, switching control signals and total control signals.

Finally, Table 1 summarizes the voltage RMS values of the disturbance, the linear, switching, and total control signals applied to PZT actuators 1 and 6. The voltage RMS value of the

nonlinear part is approximately 4 times higher than the linear part, showing that the resulting control performance and robustness still comes with power cost.

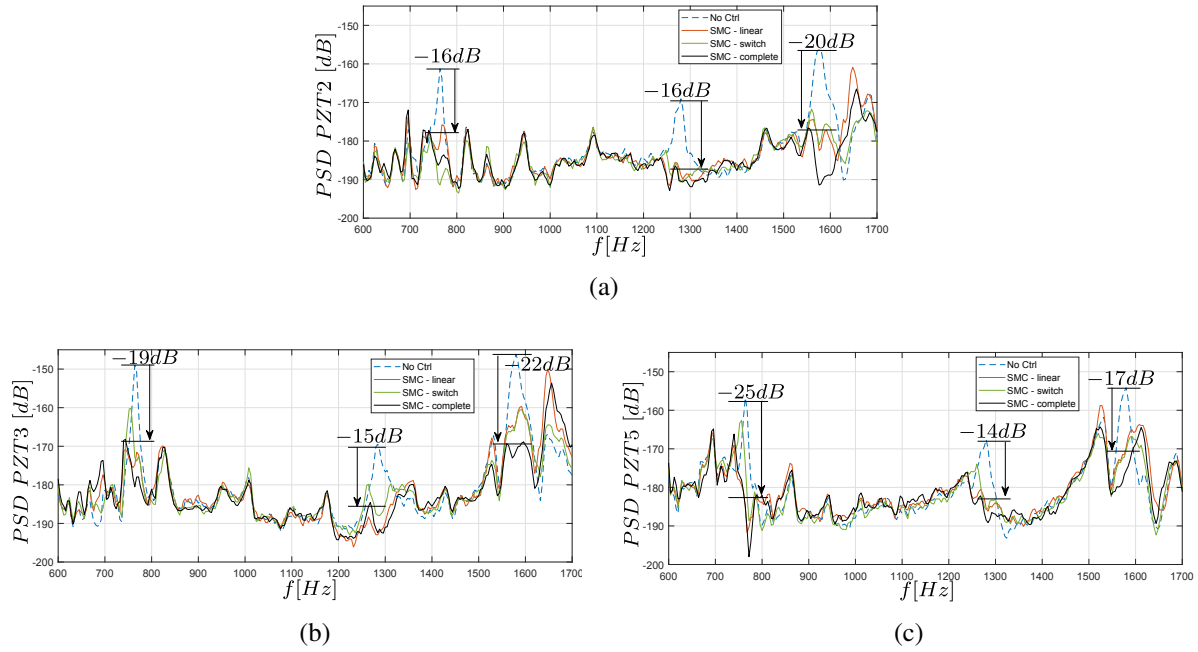

(a)

(b)

(c)

Figure 8: Experimental results: power spectral density of the PZT sensors (a) PZT 2, (b) PZT 3, (c) PZT 5.

4 CONCLUSION

Two applications of functional composite smart structures have been presented in this proceeding: an RC composite car body and a spoiler-shaped smart structure. Both structures had fully integrated piezoelectric transducers inside their fiber layers and illustrated the capabilities of composite structures to host electromechanical devices for self-sensing and dynamics control applications. In addition, the two considered smart structures show the advantage of using nonlinear switching methods for the aforementioned applications to enhance process performances and robustness. The first experiment demonstrated the viability of the energy harvesting concept using SSHI circuits to overcome the common difficulty of weak electromechanical coupling or broadband response in piezoelectric energy harvesting systems with up to 40μW recovered. For the second experiment, an SMC controller has been successfully applied to a spoiler-shaped smart composite structure. The obtained results confirm the relevance of nonlinear switching control methods for vibration mitigation. The level of performance achieved with the total control signal for each actuator went from -14dB to -22dB on three different target modes. In conclusion, the two presented applications provided concrete illustrations of the promising capabilities in the transportation field for integrated composite smart structures.

REFERENCES

[1] C. Tuloup, W. Harizi, Z. Aboura, Y. Meyer, K. Khellil, and R. Lachat, "On the use of in-situ piezoelectric sensors for the manufacturing and structural health monitoring of polymer-matrix composites: A literature review," *Composite Structures*, vol. 215, pp. 127–149, 2019.

[2] P. Shivashankar and S. Gopalakrishnan, "Review on the use of piezoelectric materials for active vibration, noise, and flow control," *Smart Materials and Structures*, vol. 29, no. 5, p. 053001, 2020.

[3] M. Safaei, H. A. Sodano, and S. R. Anton, "A review of energy harvesting using piezoelectric materials: state-of-the-art a decade later (2008–2018)," *Smart materials and structures*, vol. 28, no. 11, p. 113001, 2019.

[4] D. Guyomar, A. Badel, E. Lefeuvre, and C. Richard, "Toward energy harvesting using active materials and conversion improvement by nonlinear processing," *IEEE transactions on ultrasonics, ferroelectrics, and frequency control*, vol. 52, no. 4, pp. 584–595, 2005.

[5] E. Lefeuvre, A. Badel, C. Richard, L. Petit, and D. Guyomar, "A comparison between several vibration-powered piezoelectric generators for standalone systems," *Sensors and Actuators A: Physical*, vol. 126, no. 2, pp. 405–416, 2006.

[6] Y. Shtessel, C. Edwards, L. Fridman, A. Levant *et al.*, *Sliding mode control and observation*. Springer, 2014, vol. 10.

[7] K. David Young and Ü. Özgüner, "Frequency shaping compensator design for sliding mode," *International Journal of Control*, vol. 57, no. 5, pp. 1005–1019, 1993.

[8] A. Concha, S. Thenozhi, R. J. Betancourt, and S. K. Gadi, "A tuning algorithm for a sliding mode controller of buildings with atmd," *Mechanical Systems and Signal Processing*, vol. 154, p. 107539, 2021.

[9] Z.-c. Qiu, X.-m. Zhang, Y.-c. Wang, Z.-w. Wu *et al.*, "Active vibration control of a flexible beam using a non-collocated acceleration sensor and piezoelectric patch actuator," *Journal of sound and vibration*, vol. 326, no. 3-5, pp. 438–455, 2009.

[10] L. Yan, J. Rodriguez, K. Billon, M. Lallart, M. Collet, C. Jean-Mistral, and S. Chesné, "Energy harvesting using integrated piezoelectric transducer in a composite smart structurefor self-powered sensor applications," *Journal of Intelligent Material Systems and Structures*, p. 1045389X221121902.

[11] J. Rodriguez, M. Collet, and S. Chesné, "Active vibration control on a smart composite structure using modal-shaped sliding mode control," *Journal of Vibration and Acoustics*, vol. 144, no. 2, p. 021013, 2022.